Concept and design of a beam blanker with integrated photoconductive switch for ultrafast electron microscopy

Weppelman, I. G.C.; Moerland, R. J.; Hoogenboom, J. P.; Kruit, P.

DOI
10.1016/j.ultramic.2017.10.002

Publication date
2018

Document Version
Final published version

Published in
Ultramicroscopy

Citation (APA)
Weppelman, I. G. C., Moerland, R. J., Hoogenboom, J. P., & Kruit, P. (2018). Concept and design of a beam blanker with integrated photoconductive switch for ultrafast electron microscopy. *Ultramicroscopy*, *184*, 8-17. https://doi.org/10.1016/j.ultramic.2017.10.002

Ultramicroscopy 184 (2018) 8–17

Contents lists available at ScienceDirect

Ultramicroscopy

journal homepage: www.elsevier.com/locate/ultramic

Concept and design of a beam blanker with integrated photoconductive switch for ultrafast electron microscopy

I.G.C. Weppelman*, R.J. Moerland, J.P. Hoogenboom, P. Kruit

Department of Imaging Physics, Faculty of Applied Sciences, Delft University of Technology, Delft, The Netherlands

ARTICLE INFO

Article history:
Received 2 July 2017
Revised 30 September 2017
Accepted 5 October 2017
Available online 13 October 2017

Keywords:
Ultrafast electron microscopy (UEM)
Beam blankers
Photoconductive switches
Scanning electron microscopy (SEM)
Transmission electron microscopy (TEM)

ABSTRACT

We present a new method to create ultrashort electron pulses by integrating a photoconductive switch with an electrostatic deflector. This paper discusses the feasibility of such a system by analytical and numerical calculations. We argue that ultrafast electron pulses can be achieved for micrometer scale dimensions of the blanker, which are feasible with MEMS-based fabrication technology. According to basic models, the design presented in this paper is capable of generating 100 fs electron pulses with spatial resolutions of less than 10 nm. Our concept for an ultrafast beam blanker (UFB) may provide an attractive alternative to perform ultrafast electron microscopy, as it does not require modification of the microscope nor realignment between DC and pulsed mode of operation. Moreover, only low laser pulse energies are required. Due to its small dimensions the UFB can be inserted in the beam line of a commercial microscope via standard entry ports for blankers or variable apertures. The use of a photoconductive switch ensures minimal jitter between laser and electron pulses.

1. Introduction

Ultrafast electron microscopy (UEM) is an emerging field where the aim is to achieve sub-picosecond temporal resolution with spatial resolution in the nanometer scale. This capability enables imaging in space and time of phenomena such as spin dynamics [1], excited state dynamics [2], optical near fields [3–6], quantum optical effects [7] and motion of atoms [8]. Almost all applications of UEM rely on pump-probe experiments, where a laser pulse serves as the pump modifying the characteristics of the sample and the electron pulse probes the relaxation of the sample towards equilibrium. Thus, accurate, preferably jitter-free, locking of the ultrashort electron pulses to a laser clocking pulse is of paramount importance. Also, the repetition rate of the electron pulses should be equal to the repetition rate of the laser.

Typically, pulsed electron beams are created by modifying the source unit of an electron microscope (EM) to allow laser-triggered emission. For example, a flat photocathode illuminated with a femtosecond laser can be employed to create femtosecond electron pulses [9]. However, flat photocathodes have a low brightness. For this reason tip based photo-field emitters are used [10–12], which can have brightness values comparable to regularly used Schottky emitters [13] as measured by Feist et al. [14] and also by Dominik et al. because coherence is related to the reduced brightness [15].

A known alternative to a laser triggered source is the use of a beam blanker. Beam blankers allow both pulsed electron beam operation for time-resolved measurements and DC operation mode for normal imaging, where a user can relatively quickly switch between both modes of operation. For a laser triggered Schottky source, switching between DC and pulsed modes of operation can take up to 1 h [14]. Beam blankers based using microwave cavities to create ultrashort electron pulses were envisioned and realized by Oldfield [16] and Ura and co-workers. In this way, electron pulses of 200 fs were created [17]. At that time, the electron pulses were used to measure switching speeds in electronic circuits and transistors by means of voltage contrast [18,19]. Lassise et al. and van Rens et al. calculated that a TEM_{110} cavity positioned conjugate to the electron beam focal point is able to create ultrashort electron pulses while maintaining the brightness of the continuous electron beam, recently such a TEM_{110} cavity is incorporated in a commercial TEM [20–22]. Advances in technology now allow synchronization between an RF microwave cavity and a laser clock pulse to values of 100 fs and shorter, where additionally care has to be taken to match the GHz microwave frequency to typical MHz laser repetition rates [23,24]. Beam blanking triggered by a laser clocking pulse would directly and in a straightforward way synchronize electron and laser pulses.

Here, we present such an approach to create ultrafast electron pulses with a laser-triggered beam blanker. In our concept fem-

* Corresponding author.
E-mail addresses: j.p.hoogenboom@tudelft.nl, i.g.c.weppelman@tudelft.nl (I.G.C. Weppelman).

https://doi.org/10.1016/j.ultramic.2017.10.002
0304-3991/

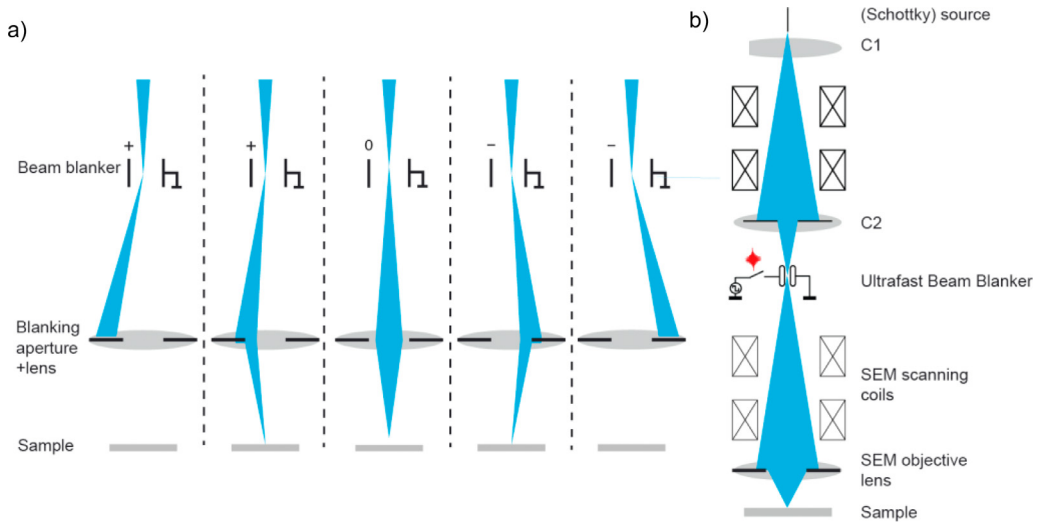

Fig. 1. (a) Schematic drawing indicating conjugate beam blanking using an electrostatic deflector to sweep the electron beam over a blanking aperture. The deflector is in a conjugate plane with respect to the image/sample plane to ensure that the electron probe is always at the same location at the sample irrespective of the electric field strength in the deflector, neglecting abberations of the objective lens. (b) System overview of a commercial SEM, which can have a high brightness Schottky electron source. C1 and C2 denote condenser lenses to focus the electron beam between the blanker plates. The UFB is positioned at the standard entry port for blankers or variable apertures.

tosecond electron pulses are achieved through a combination of an electrostatic beam blanker and a photoconductive switch illuminated with femtosecond laser pulses [25]. The use of a photoconductive switch enables miniaturization of the ultrafast beam blanker (UFB) such that it can be directly inserted in an existing, commercial EM. Also the UFB is jitter-free locked to the laser pulse, essential for achieving electron pulses deep in the femtosecond time range. We will first present the concept of our UFB and discuss the basic requirements for realization. We will then turn more in-depth to the requirements on the photoconductive switch and physical properties of available materials, which leads to a set of parameters for the actual design. Based on these we derive the spatial and temporal resolution that could be achieved with such a design. This shows that electron pulses in the 100 femtosecond time range with sub-10 nm spatial resolutions may be feasible.

2. UFB concept and requirements

Electrostatic beam blankers are commonly used in EM's to ensure that the sample is exposed to the electron beam only when demanded, for example for electron-beam lithography. In such a blanker the electron beam is deflected and then blocked by an aperture. The preferred position for the blanker is in a plane conjugate to the image plane located at the sample, as indicated in Fig. 1 [26,24]. This ensures that the position of the electron spot is at a steady position at the sample while the blanker deflects the electron beam. We want to use this same concept to generate femtosecond electron pulses, sweeping the electron beam over an aperture in (sub-) picosecond time scales.

A first requirement for our beam blanker is that the electron beam sweeps back and forth over the aperture at (sub-)picosecond timescales. Obviously, this needs inversion of the voltage over the deflector. As we want to synchronize the electron pulses to the output of a femtosecond laser (see details later), another important requirement is that the electron pulses are generated at a rate equal to the repetition rate of the laser. In order to sweep the electron beam ultrafast over the aperture in both positive and negative direction, we propose the innovative scheme shown in Fig. 2.

By electrically connecting the photoconductive switch and beam deflector in series, the voltage at the feed plate can be inverted each time the switch has been illuminated with the laser pulse. For this to be possible the photoconductive switch has to return to its insulating state after laser illumination on a timescale fast compared to the interval between the laser pulses. In that case the voltage at the feed plate can be inverted while the voltage at the deflector plate remains constant. This then ensures that the electron beam is swept over the blanker aperture in opposite directions for consecutive laser pulses. Hence, below the blanking aperture we will generate electron pulses at a repetition rate equal to the femtosecond laser system.

To increase the average current in the pulsed electron beam, it is advantageous to work at highest possible laser repetition rates, in practice about 100 MHz. This requirement limits the pulse energy available for operating the photoconductive switch to the nanojoule range, as this is the typical operation energy for high repetition rate femtosecond lasers.

For pump-probe measurements with a laser and electron pulse the temporal resolution is not only set by the electron pulse length but also by the amount of jitter between the laser pulse and electron pulse. The latter requirement of minimal jitter is relatively easily satisfied because we use a photoconductive switch illuminated with a laser pulse to change the deflection voltage at the beam blanker. In other words there is a direct link between the laser pulse and the change in voltage. A minimal amount of timing jitter is still present, we will discuss this at the end of the paper.

In general, for photoconductive switches, a short recombination time is important to generate short voltage pulses. However, in our case this is not important, because we directly connect the photoconductive switch to the beam blanker (see Fig. 2) and only use the rising part to charge the deflector plate and sweep the beam. When the laser illuminates the photoconductive switch, electrons are excited to the conduction band, and, under influence of the bias electric field, diffuse to the blanker plate and (de)charge it.

Finally, to create ultrashort electron pulses with the concept discussed here, it is essential that photoconductive switch and deflector have a short response time. For this reason we discuss the physical processes occurring in the photoconductive switch and resulting implications for the design in the next paragraphs. We start with a short literature discussion that shows that photoconductive switches are known to have ultrashort response times. We then discuss the requirements on the semiconductor material to be used

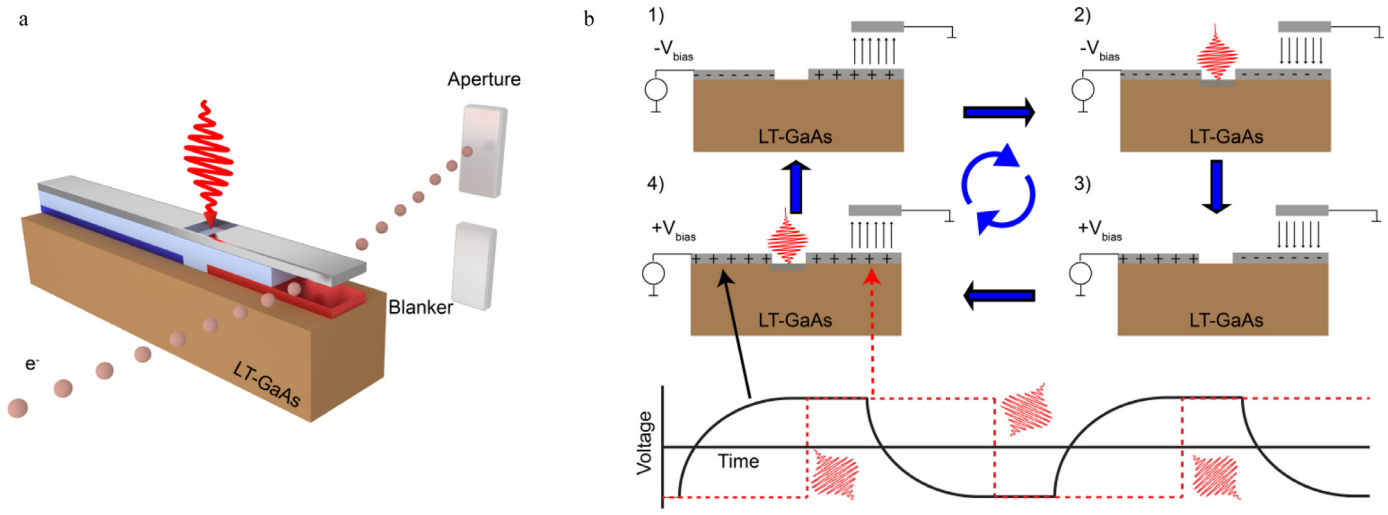

Fig. 2. (a) Schematic indication of our UFB concept: a photoconductive switch is connected to an electrostatic beam blanker, the electron beam is deflected and intercepted by an aperture, the colors of the electrodes indicate +10 V (blue), negative −10 V (red) and ground (grey). (b) Full modulation cycle for the UFB: (1) the beam is initially blanked by the deflection field in the blanker; (2) laser irradiation provides a conductive channel in the GaAs wafer inverting the voltage on the deflector and thus the deflection direction; (3) after the laser pulse, the GaAs restores to its insulating state, subsequently the bias on the feed voltage from the supply line is switched; (4) a next laser pulse again inverts the field in the deflector, sweeping the beam in opposite direction, after which the voltage supply inverts again and the modulation cycle is back to the initial situation. (For interpretation of the references to colour in this figure legend, the reader is referred to the web version of this article.)

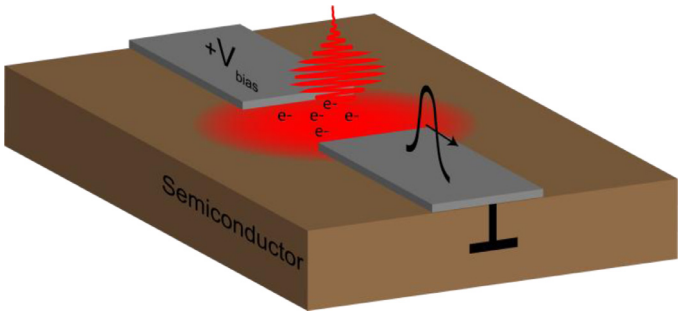

Fig. 3. Basic principle of a photoconductive switch. Two conductors are connected via an isolating semiconductor material, a laser pulse creates free carriers to provide a conductive channel between the electrodes. Due to recombination of e-h pairs and/or diffusion of electrons and holes to the metal electrodes the conductivity will decrease again after illumination with the laser pulse.

and subsequently calculate the achievable conductivity in and field strengths over the switch. Based on the photoconductive switch design requirements the dimensions of the beam deflection unit can be calculated, which we show in paragraph 5. Then, in paragraph 6, we provide an estimation of the achievable electron pulse length for the set of parameters required for the design. We also estimate the amount of jitter of the electron pulse with respect to the laser pulse in paragraph 7. The paper ends with a conclusion and discussion of the concept and results.

3. Photoconductive switch

In the above concept, a photoconductive switch is used to create an ultrafast voltage ramp. A photoconductive switch basically consists of a semiconductor material in between two metal contacts, see Fig. 3. In the literature, such a device is also called an Auston switch, named after the inventor [27].

Photoconductive switches creating 825 V pulses with 1.4 ps rise time have been demonstrated [28], and fast photoconductive switches with >100 GHz bandwidth have also been demonstrated [29]. Photoconductive switches are also commonly used to generate THz pulses [30]. Photoconductive switches are also employed to create streak cameras to characterize electron pulses [31] and for X-ray streak cameras [32]. Most photoconductive switches are made of the direct band-gap semiconductors GaAs or LT-GaAs, the latter consisting of a special top layer of GaAs grown at a lower temperature [33]. These two semiconductor materials have the highest conductivity under laser illumination. LT-GaAs has a somewhat lower conductivity under laser illumination compared to GaAs but a shorter carrier recombination time, of the order of 1 ps while normal GaAs has a recombination time of about 1 ns [34]. In applications where short voltage pulses are required, LT-GaAs is the preferred choice, because the voltage pulse length is limited by the carrier lifetime.

For the UFB only the rising part of the photocurrent is important, as this determines the time to charge the deflector plate. However, as discussed above and indicated in Fig. 2, the photoconductive switch also has to return to the insulating state comparatively fast to be able to modulate the voltage at the feed plate. Otherwise, the voltage at the deflector plate, indicated with the red dotted line in Fig. 2, will be affected when the voltage at the feed plate is inverted. Hence, to sufficiently isolate the deflector and feed plate the dark resistance, $R_{s,off}$, has to obey the following inequality:

$$R_{s,off} C_{blanker} > \frac{1}{f} \quad (1)$$

where $C_{blanker}$ is the capacity of the deflector plate and f is the repetition rate of the laser. In the following paragraphs we will argue that the capacitance of the deflector plate has to be lower than 10 fF. A typical Ti:Sapph laser has a repetition rate, of about $f = 100$ MHz, lower repetition rates are not attractive because the average probe current will be reduced, as mentioned in the previous paragraph. Hence, high values of the dark resistance are required, of the order of 10^6 Ω range. This in turn requires a relatively short recombination time. For this reason it is not preferred to use regular, 1 ns recombination time, GaAs for the photoconductive switch, but LT-GaAs instead. For experiments where a low repetition rate is required, the repetition rate of the electron pulse can be reduced by switching the feed plate voltage, indicated in Fig. 2b, at half the desired repetition rate for the electron pulses.

3.1. Response time photoconductive switch

We will now discuss the conductivity values that can be achieved and the electric field strength that can be maximally ap-

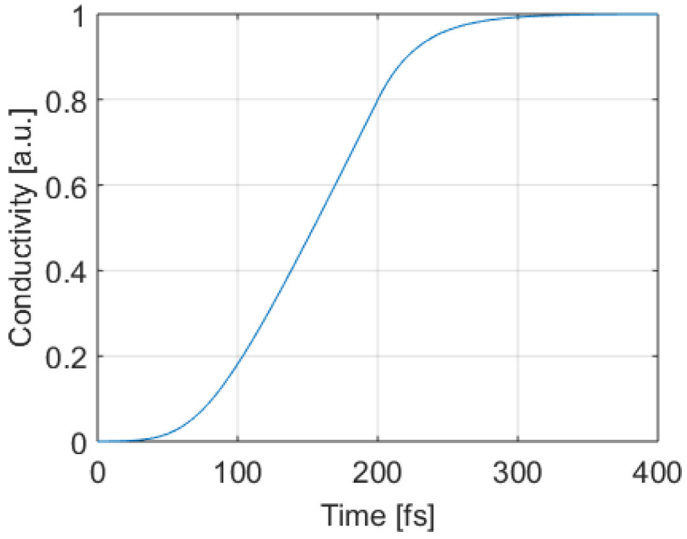

Fig. 4. Conductivity in the photoconductive switch as function of time for illumination with a Gaussian laser pulse of 50 fs duration and a scattering time in the semiconductor of 30 fs. The calculation is based on a Drude–Lorentz model for the average electron drift velocity, Eq. (2), convoluted with a typical 50 fs FWHM Gaussian laser pulse. It takes approximately 100 fs to build up conductivity in the semiconductor.

plied over the photoconductive switch. Hereto, we first consider the physical processes occurring in the photoconductive switch after and during illumination with a femtosecond laser pulse, based on a Drude–Lorentz model.

Upon laser illumination, electron hole pairs are created in the photoconductive switch provided the photon energy is larger than the bandgap. We assume that every photon in the pulse creates an electron hole pair with the same probability, determined by an absorption coefficient and a quantum efficiency. Initially, electron and hole will be at 'rest' followed by acceleration in the electric field. The average electron velocity, v, is described by Newton's 2nd law:

$$\frac{dv}{dt} = \frac{e}{m*}E - \frac{v}{\tau_s} \tag{2}$$

where m^* is the effective mass of the electrons, equal to 6.7% of the electron rest mass, E is the local electric field, τ_s is the momentum scattering time, equal to about 30 fs [35]. The scattering term describes the loss of kinetic energy due to collisions of the free carriers with the lattice. The electric field consists primarily of the voltage applied on the electrodes but can be partially screened by surrounding free charges. We note that each electron also has a random thermal motion, but Eq. (2) describes the net average velocity opposite the direction of the electric field.

With the average velocity we can calculate the current density in the semiconductor:

$$j = nev = \sigma E \tag{3}$$

where n is the free carrier density and σ the conductivity. We assume a constant or slowly changing electric field E, and convolve the solution of Eq. (2) with a Gaussian laser pulse, with a typical length of 50 fs FHWM, to find how the conductivity in the semiconductor develops in time. The result is given in Fig. 4, which shows that the conductivity builds up in about 100 fs.

We don't take into account negligible nonlinear effects like optical rectification inducing displacement currents at terahertz frequencies. Note that there is also another instantaneous effect on the conductivity, which we did not take into account in calculation the result in Fig. 4: the laser illumination will lead to a polarization in the semiconductor material which in turn will induce a bound current. However, from literature, this is known to give a negligible contribution to the current at high bias fields [36,37].

3.2. Electric field strength over the photoconductive switch

In the Drude–Lorentz model, the charge carriers at some point reach their so-called drift velocity, v_d, the maximum average velocity due to collisions with each other and the lattice:

$$v_d = \mu E \tag{4}$$

where μ is the mobility, about 0.3 $m^2V^{-1}s^{-1}$ for LT-GaAs [34,38]. For example, with a field strength of 2 MV/m, the drift velocity will be $1.6{\cdot}10^5$ m/s according to the Drude–Lorentz model and parameters used in Eq. (2). At low fields the temperature of the charge carriers is equal to the lattice temperature, but at higher fields the carrier temperature begins to deviate from the lattice temperature. Then, the drift velocity no longer increases linearly with the field and starts to saturate. In GaAs, the saturation velocity is about $2{\cdot}10^5$ m/s [39], which is slightly above the drift velocity at 2 MV/m. Note that the thermal velocity of conduction electrons is about $3.7{\cdot}10^5$ m/s.

Thus, for an electric field of 2 MV/m, we can assume a linear relation between bias voltage and current. We will use this value in the remainder of this paper. In principle it is possible to further increase the bias voltage, but other effects like impact ionization and voltage breakdown may then happen. In addition, in III-V compounds, like GaAs, the electron mobility also decreases with increasing field due to scattering of electrons by optical phonons. It has been shown experimentally that the photocurrent increases at a slower rate at higher fields [35].

3.3. Conductivity photoconductive switch

Eq. (3) may seem to imply that a higher laser power induces a larger photocurrent and conductivity. However, it should be noted that at relatively high free carrier densities oscillations in the photocurrent may be induced. As the laser creates a plasma of free carriers in the semiconductor material, electrons and holes in the plasma will separate due to the applied electric field. Due to the resulting Coulomb forces the plasma may start oscillating and/or the photocurrent may decay very rapidly. A laser pulse shorter than the momentum scattering time can also lead to these oscillations. In Jepsen et al., these effects are explained in detail and fitted to measurements [35]. It is shown that the onset of plasma oscillations is determined by the product of the scattering time and the plasma frequency, defined as:

$$\omega_p = \sqrt{\frac{ne^2}{\varepsilon m^*}} \tag{5}$$

where ϵ is the permittivity. We would enter the regime where these oscillations start to occur at $a = \omega_p\tau_s \sim 1$. Therefore, we want to have a density of free carriers equal to:

$$n = \frac{a^2\varepsilon m^*}{e^2\tau_s^2} = 1.15 \cdot 10^{24}[\mathrm{m}^{-3}] \tag{6}$$

where we assume a value 12.3 for the relative permittivity and for the product of $\omega_p\tau_s$, we took a value of a equal to 2. Note that there is a difference between the situation described by Jepsen et al. and our design, as in their case the electric field over the switch is constant.

To conclude this section, a carrier density of about $1{\cdot}10^{24}$ m^{-3} should be achievable in combination with an electric field of 2 MV/m over the photoconductive switch. The switch can be brought in the conductive state in about 100 fs, later we will give more accurate values where we take into account the change in

electric field over the photoconductive switch. In the next paragraph we will discuss the dimensions required for the photoconductive switch.

4. Transmission of high frequency signals and implications for the design

We have seen above (see Fig. 4) that the conductivity of the photoconductive switch will change on time scales smaller than 1 ps. This corresponds to terahertz-range frequencies. Transmission of electrical signals with such high frequency components to the deflector is not trivial: Normally for electronics, it is assumed that the potential along a perfect conductor is independent of position even when the potential is time-dependent. However, electrical signals are transferred at the local speed of light. So, when the signal delay, as determined by the length of the cable and its effective permittivity, becomes comparable to 0.1 times the signal rise time, the potential becomes position dependent.

In *vacuum*, a 1 ps electromagnetic wave has a wavelength of 300 µm, a line longer than 30 µm will behave like a transmission line. In our case we also have to consider that we have a broadband signal while the response of the electrical circuit can be strongly wavelength dependent. In addition, dispersion may reduce the rise time of the electrical signal. Another issue is that high-frequency signals are absorbed quite strongly by metals due to the low skin-depth and finite conductivity.

Finally, an essential requirement is that the amount of charges necessary to charge or discharge the deflector plate has to be less than the amount of charges created by the laser pulse. Because when all free charges (created by the laser pulse) are taken up by the electrodes the resistance of the photoconductive switch is equal to the initial dark resistance and the photocurrent will drop to zero.

We choose a photoconductive switch with dimensions of 10 by 10 µm because it is only a fraction of the wavelength and because the field is set to 2 MV/m, see section paragraph 3.2, resulting in a voltage difference of 20 V over the photoconductive switch which is relatively easy to achieve with standard pulse generators in a few nanoseconds. Under those conditions, we would generate $\sim 10^8$ free carriers, taking into account the required carrier density calculated in Section 3.3 and assuming a skin depth of 1 µm. This means the maximum capacitance we can switch is equal to 8 pF for a 20 V difference. The required laser power is low: with an 800 nm femtosecond laser at a repetition rate of 100 MHz, 5 mW is required, excluding losses.

To summarize, the capacitance that can be connected to the photoconductive switch is limited. Together with the need to reduce absorption, dispersion, and transmission line behavior, this translates to photoconductive switch dimensions of the order of ten micrometers. Therefore, we choose to integrate the photoconductive switch and the deflector in a single MEMS-sized device.

5. Dimension MEMS beam blanker

In the previous paragraph we discussed that the photoconductive switch and deflector should be integrated in a single MEMS sized device. From this requirement and the required sub-10 nm spatial resolution we can calculate typical dimensions for the deflector.

The deflection angle can be calculated from the dimensions of the blanker using the following equation (see also Fig. 6):

$$\alpha_b = \frac{El}{2\phi} = \frac{V_b l}{2\phi d} \tag{7}$$

where E is the electric field between the deflector plates, V_b the voltage difference over the deflector plates and ϕ is the acceleration voltage. All other variables are defined in Fig. 6. The two requirements for blanking are:

$$\begin{aligned} &\alpha_b > 2\alpha \\ &d > d_g + \alpha l \end{aligned} \tag{8}$$

where d_g is the diameter of the focused spot between the deflector plates, i.e. the crossover diameter. The first requirement states that we have to deflect at least an angle α_b to have the beam completely blocked by the aperture. The second requirement states that the beam should not hit the deflector plate.

Eq. (8) tells that the blanking angle will be determined by the half opening angle. In electron microscopy, the choice of half-opening angle α_b is a balance between spatial resolution and probe current. A higher opening angle leads to a larger current but at the cost of spatial resolution due to increasing lens aberrations, except at very low opening angles where diffraction can become dominant. With our beam blanker, the current at the sample will be reduced significantly compared to continuous beam operation. Therefore, in the remainder of this section we will work with a high beam current of 16 nA. For 100 fs electron pulses and a repetition rate of 100 MHz, this will result in a duty cycle of $1{\cdot}10^{-5}$. With this 16 nA DC current, every electron pulse will on average contain 0.01 electron.

With the 16 nA current, and considering the probe size limited by spherical aberration and source to image plane magnification, the probe size at the sample is given by [40]:

$$I_p = 2.47 \frac{d_p^{8/3} B_r \phi}{C_s^{2/3}} \tag{9}$$

where we assume a reduced brightness $B_r = 5{\cdot}10^7$ A/m^2·sr·V and $C_s = 15$ mm. Notice that we a spherical aberration coefficient for a non-immersion lens, in a system with an immersion lens the spherical aberration coefficient will be lower and subsequently the probe will be reduced. The acceleration voltage, ϕ, is taken to be equal to 30 kV to obtain highest spatial resolution and because at lower beam energies the electron pulse length will increase more due to the energy spread within the pulse. The effects of energy spread will be discussed in detail in the next paper. With the numbers stated above, we see that for a DC current of 16 nA, a spot size of 8.3 nm can be obtained.

With the geometrical part of the spot size at the sample we calculate a FW50 value of 200 nm for the spot size at the blanker, d_g, for a sample to deflector magnification of 30. The opening angle at the blanker can be calculated using conservation of brightness:

$$\alpha_p = \sqrt{\frac{4I_p}{B_r \pi^2 \phi}} \frac{1}{d_g} \tag{10}$$

This results in a half-opening angle of 0.32 mrad.

To be able to design the deflector we have to estimate the product of the blanking voltage V_b and blanker length l which can be calculated as:

$$V_b l > 2\phi \alpha_b d = 38.9 \cdot 10^{-6} [\mathrm{V} \cdot m] \tag{11}$$

with a separation between the deflector plates, $d = 1$ µm, and $\alpha_b = 0.32$ mrad. The separation between the deflector plates is chosen to be in micrometer-range for two reasons. The first one is that the distance between the electrode containing the signal and the ground plate is preferred to be (deep) subwavelength. The second reason is that with smaller separation, the electric field will be maximized which reduces the required length and blanking voltage. Note that the blanking voltage has to be lower than the maximum deflection voltage that we can deliver with the photoconductive switch, which was 10 V as discussed in the previous paragraph. Also, even smaller distance between the plates is difficult

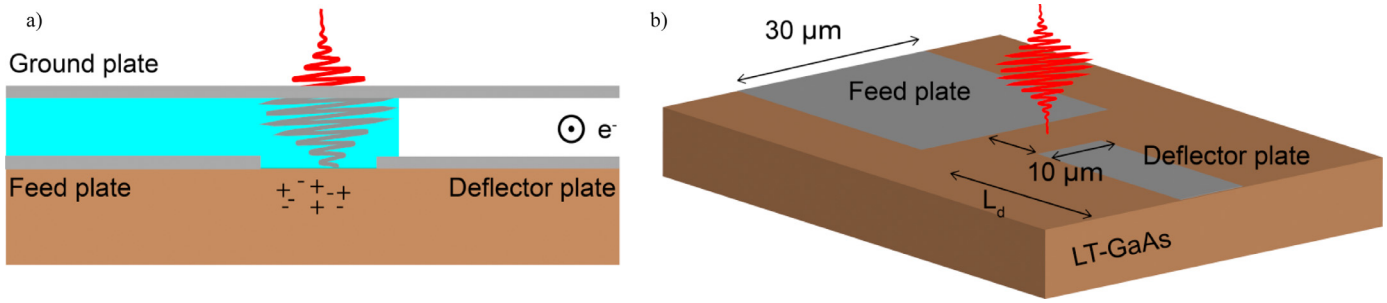

Fig. 5. (a) Sketch of the photoconductive switch with feed, ground, and deflector plates. The electron beam traverses the space between the ground and deflector plate perpendicular to this plane. (b) View of the LT-GaAs plane from (a), with feed and deflector plates. The photoconductive switch is 10 by 10 µm as discussed in the text. The feed plate is 30 µm wide to assure that locally enough charges are present to charge the deflector plate when the photoconductive switch is in the conductive state.

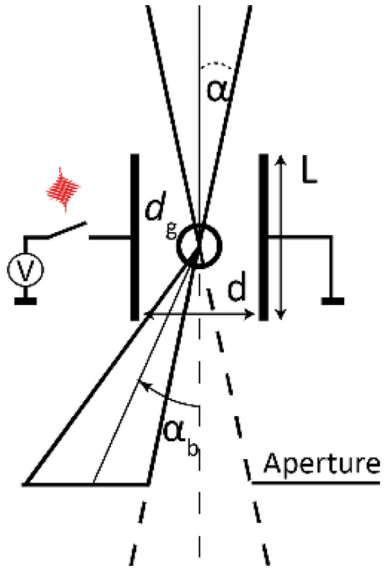

Fig. 6. Sketch of a beam blanker. The incoming electron beam has a half-opening angle α and has a crossover of diameter d_g between the deflector plates. The deflector has a length l and the plates are separated by a distance d. The deflector sweeps the beam over an aperture. α_b is the smallest deflection angle with which the beam is completely blocked by the aperture.

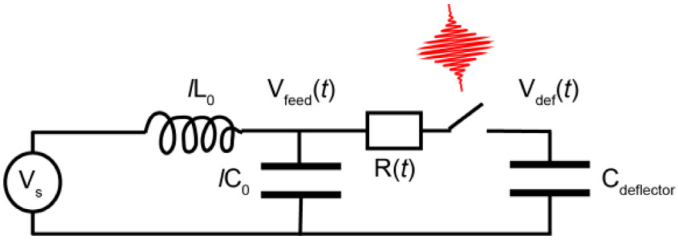

Fig. 7. Schematic of the electrical circuit used. With a set of differential equations the time-dependent voltage at the feed plate, $V_{feed}(t)$, and at the deflector plate $V_{def}(t)$ is calculated. The voltage delivered by the source, Vs, is constant. The resistance of the photoconductive switch, R(t) is time-dependent. Also the Drude model and a laser pulse duration of 25 fs is taken into account.

because the system becomes more sensitive to drift and mechanical stability and is also limited by the 200 nm spot diameter of the electron beam in the blanker. Finally, we note that a deflector with an aspect ratio larger than 1:10 will be more difficult to align with respect to the electron optical axis. We then see that for a 10 µm long deflection plate, a blanking voltage of 3.8 V is required.

6. Electron pulse length

With the dimensions of the blanker and the blanking voltage set, we can estimate the electron pulse length. Hereto, we need a calculation for the time-dependent voltage at the deflector plate. Two approximations in this section are described to calculate the electron pulse length. In the first approximation we consider the photoconductive switch as a resistor and the deflector as a capacitor and we calculate the RC time.

From the conductivity, calculated in Section 3.3, a mobility of 3000 $cm^2/V{\cdot}s$, and skin-depth of 800 nm light in GaAs of 1 µm, the resistance of the photoconductive switch is about 18 Ω. The deflector plate, indicated in Fig. 5, can be approximated as a parallel plate capacitor with a capacitance of 6 fF, neglecting parasitic capacitances. Where it is assumed that the area is equal to $l{\cdot}L_d = 300\ \mu m^2$, and the plate separation is 1 µm in combination with a relative permittivity of 2.25 due to the presence of glass. Hence the RC time is about 110 fs, in combination with a conductivity built-up of about 100 fs, shown in Fig. 4, and square addition the electron pulse length will be in the order of 150 fs.

In the RC time calculation the response of the photoconductive switch is not considered. In reality the photoconductive switch has a non-zero response time as described by the Drude–Lorentz model in Eq. (2). Also the electric field over the photoconductive switch depends on time after illumination.

For this reason, we performed a second approach which also takes into account the response time and the time-dependency of the conductivity. We implement a time-dependent field over the photoconductive switch by modeling the transmission line between constant voltage source and photoconductive switch with an inductor L_0 and capacitor C_0 (Fig. 7), Also, we take a time-dependent resistance of the photoconductive switch using the Drude–Lorentz model described in Section 3.1. Finally, the finite duration of the laser pulse is taken into account using a Gaussian pulse shape with 25 fs FWHM. In this way, we derive a set of differential equations, as detailed in the Appendix A. These are numerically solved with MATLAB. A scattering time τ_s of 30 fs is assumed for this calculation which corresponds to a mobility of 786 $cm^2/V{\cdot}s$, the exact mobility and scattering time do depend on, for example, the annealing time of the LT-GaAs layer [34]. The results of the calculation are shown in Fig. 8, all values used in the calculations are listed in the Appendix A.

In Fig. 8b we can see that the FW50 electron pulse length increases when the carrier density decrease, but that this does not occur in the simple linear relation predicted by the bare RC model. One reason for this is that in the time-dependent model, the response of the switch becomes limited by the acceleration of free carriers.

Fig. 8c clearly shows that the pulse length strongly depends on the capacitance of the deflector plate. A low value for the capacitance results in a short electron pulse length. However, as stated

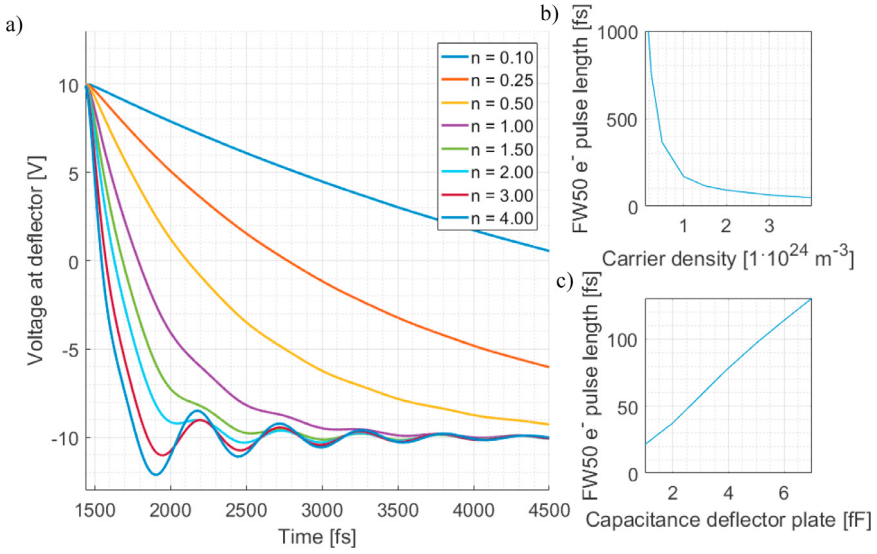

Fig. 8. (a) Calculated voltage at the deflector plate as function of time for different free carrier densities n in [$1{\cdot}10^{24}$ m^{-3}]. At high carrier densities oscillations occur which has to do with the delay in the supply of charges at the feed plate. (b) The FW50 electron pulse length increases with lower carrier density. In (a) and (b) the capacitance of the deflector is 6 fF. (c) FW50 electron pulse length as function of the feed plate capacitance, for a fixed carrier density of $1.5{\cdot}10^{24}$ m^{-3}. In the calculations, the voltage at which the electron beam is fully blanked is assumed to be 3.8 V.

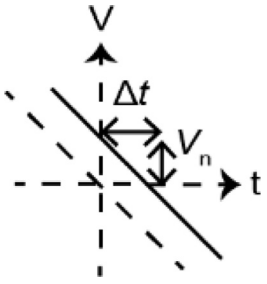

Fig. 9. Voltage over the deflector as function of time in case without noise, dotted line, due to voltage noise, V_n, the graph moves to the right, solid line, the zero crossing by an amount Δt. Hence the electron pulse is also shifted by an amount of Δt.

before (see, e.g., Eq. (1)), a low capacitance also reduces the RC time in the dark state of the switch. For too low capacitance, it will become impossible to invert the voltage at the feed plate between two subsequent laser pulses while keeping the voltage at the deflector plate constant. A typical dark resistance is measured to be in the 10 MΩ range, resulting in a RC time of 10 ns for a 1 fF deflector. This is too low for a laser repetition rate of 100 MHz.

The electron pulse length depends linearly on the capacitance of the deflector plate, as shown in Fig. 8c. Analytical equations to estimate the exact capacitance of a 3D geometry with different dielectric materials around the deflector are not available. We will discuss this further in the subsequent paper were we performed numerical simulations of the UFB.

7. Time jitter between the laser pulse and the electron pulse

In the previous section we have calculated that electron pulses in the 100 fs range are feasible. However, the temporal resolution in a UEM is not only determined by the electron pulse length but also due to time jitter between the laser pulse envelope and the electron pulse. The jitter is present because the photoconductive switch converts an optical signal, the laser pulse, to an electronic signal which has some noise. The noise on the voltage will converted to time jitter due to a time shift in the zero crossing of the deflector voltage (Fig. 9).

We consider two contributions to the jitter; thermal noise and shot noise. Firstly the latter contribution is estimated, the rms shot noise current is given by:

$$I_{shot} = \sqrt{2eI_{avg}\Delta f} = \sqrt{\frac{2en_f I_{avg}}{\tau_0}} \tag{12}$$

where I_{avg} is the average current and Δf is the bandwidth. The bandwidth is equal to a factor n_{f} times the inverse of the time constant τ_0 of the system. The power spectral density of shot noise is constant as long as the frequency is smaller than $1/\tau_{\mathrm{e}}$, where τ_{e} is the pulse width of a one electron pulse.

The average current, I_{avg}, through the capacitor is calculated as follows:

$$\begin{aligned} I(t) &= C_{def}\frac{dV}{dt} = 2\frac{C_{def}V_0}{\tau_0}\exp(-\tau/\tau_0) \\ I_{avg} &= \frac{C_{def}V_0}{4\tau_0^2}\int_0^{4\tau_0}\exp(-\tau/\tau_0)d\tau \approx \frac{C_{def}V_0}{2\tau_0} \end{aligned} \tag{13}$$

where we estimate the deflector is exponentially charged with a time constant τ_0. The average current I_{avg}. is calculated by integrating the current over a time window of $4\tau_0$. The shift in charging time is approximated as:

$$\Delta t \approx \frac{I_{shot}}{I_{avg}}\tau_0 = 2\sqrt{\frac{qn_f}{V_0C_{def}}}\tau_0 \tag{14}$$

When a time constant of 300 fs, a deflection voltage of 10 V and a capacitance C_{def} of 7 fF and a n_{f} of 3 (corresponding to a 10 THz bandwidth) is assumed, the shot noise jitter contribution is about 1 fs.

Jitter is also introduced by thermal agitation of charge carriers, as discussed by Nyquist [41]. Thermal voltage noise over a capacitor can be calculated with the equipartition theorem and is equal to [42]:

$$v_n = \sqrt{\frac{kT}{C_{def}}} \tag{15}$$

where k is Boltzmann's constant and T the temperature. The drop of thermal noise at high frequencies, around 1 THz, is neglected. From Eq. (15) the time jitter, due to thermal noise, is calculated as:

$$\Delta t \approx \frac{v_n}{V_0}\tau_0 = \frac{1}{V_0}\sqrt{\frac{kT}{C_{def}}}\tau_0 \tag{16}$$

For a temperature of 300 K, and all other parameters equal to the values used for the shot noise jitter contribution, a value of 23 as is obtained.

Amplitude noise in the laser will induce noise in the photoconductivity and hence jitter in the electron pulse. In a model where the conductivity of the switch varies linearly with the amount of photons in the pulse, the resulting time jitter for a relative laser amplitude noise η is equal to:

$$\Delta t = t_0 ln(2)\eta \quad (17)$$

For a laser amplitude noise of 0.05% RMS over a bandwidth from 10 Hz the jitter is about 10 as, for longer time scales the power stability is some 0.5% resulting in a time drift of about 1 fs. The latter contribution is only relevant for measurements who require long integration times. The rms amplitude noise and power stability are typical for a Coherent Vitara Ti: Saphh oscillator.

Thus the dominant source of jitter is shot noise which is in the order of 1 fs, so the time jitter is negligible to the electron pulse duration of 100 fs. The amount of time jitter is also significantly lower compared to systems employing GHz cavities, for example Brussard et al. achieved 96 fs time jitter and more recently Gliserin et al. reduced the timing jitter to 4 fs [23,24].

In reality the jitter will be larger as the mechanical and thermal stability of the whole setup is essential, mechanical vibration amplitudes in the optical setup will easily add a few femtosecond of jitter. Nevertheless, the amount of jitter can be expected to be significantly smaller than the electron pulse length.

8. Discussion

The above considerations and modeling have demonstrated the feasibility of operating an UFB based on a laser-illuminated photoconductive switch. In the calculations several idealized assumptions are made, for instance ideal electrical contacts to the photoconductive switch, no parasitic capacitances, no leakage current except through the photoconductive switch.

In our calculations, we have worked with a relatively high DC current of 16 nA in order to optimize the average number of electrons per pulse. A higher brightness electron source or a lower desired current will lead to (significantly) smaller opening angles and hence higher spatial resolution and shorter electron pulses. We have been conservative by assuming a reduced brightness value of $5{\cdot}10^7$ A/[$m^{2}{\cdot}$sr·V]. A factor 4 higher can be achieved with a Schottky emitter as shown by van Veen et al. [43]. This would reduce the blanking voltage by a factor of 16 for the same DC current and probe size. Hence, the exact design of the UFB can depend on the EM to be used and for some application lower currents might be acceptable.

The resistance of the photoconductor in its photoconductive state can be adjusted by setting the amount of photons per laser pulse. With fewer photons per pulse, the rise time of the deflection field would decrease. This can be used to increase the pulse length and thus also increase the current for experiments where a lower temporal resolution is acceptable. If required, the repetition rate of the electron pulse can be reduced by inverting the voltage at the feed plate at a rate lower than the laser repetition rate.

The concept of a MEMS-based UFB presented here would in principle be applicable to any type of EM because of its small dimensions. This way constitute a unique advantage compared to other UFB concepts, such as GHz resonant cavities [44,45]. The MEMS sized device could be inserted via a standard EM entry ports used for aperture strips and regular pico- to nanosecond scale beam blankers [46]. At the same time, all DC imaging modalities are kept intact because neither the high brightness electron source nor the column is modified. Also, an EM equipped with a UFB can be switched between pulsed and DC operation without any realignments. In this paper we assumed that the UEM would be used in an imaging mode where the sample and UFB are in conjugate planes. For some imaging techniques like Lorentz microscopy and holography, this is not possible. The effects of sweeping the beam, such as a possible reduction of transverse coherence or a correlation between the spatial domain and the time within the electron pulse will be discussed in a separate paper.

Fabrication of the MEMS sized UFB is in principle possible by using nanotechnology tools such as standard lithography, deposition and etching tools. Currently we have fabricated such a MEMS sized UFB and we are currently testing the performance of the device in a SEM.

9. Conclusion

In this paper, we have presented a new concept for an ultrafast beam blanker using a combination of an electrostatic deflector connected in series with a photoconductive switch. We have demonstrated the feasibility of this concept based on a design that followed from basic, practical requirements for operation of such an UFB in a standard EM. A crucial aspect of our design is that only the rising part of the signal from the switch is used to invert the voltage over the deflector at sub-picosecond time scales. By inverting the voltage at the feed plate in between laser pulses, it is possible to scan the electron beam over a blanking aperture at ultrafast time scales. By integrating the photoconductive switch with a beam blanker the dimensions can be kept substantially smaller than the wavelength and the capacitance can be reduced, enabling inverting the deflector voltage at (sub-) picosecond time scales. According to our basic models, 100 fs electron pulses with spatial resolution of less than 10 nm can be achieved. Moreover, as the electron beam is only transmitted through the blanking aperture when a laser pulse illuminates the photoconductive switch, there will be minimal jitter (only about 1 fs) between the laser pulse and electron pulse. Our calculations have shown that all dimensions of the UFB need to be micron scale to prevent transmission line behavior, dispersion and absorption of the high frequency signal components, which is feasible with MEMS fabrication technology. Our concept for an UFB may provide an attractive alternative to do ultrafast electron microscopy, as it does not require modification of the microscope nor realignment between DC and pulsed mode of operation.

Acknowledgements

This work is part of the research programme of the Foundation for Fundamental Research on Matter (FOM), which is part of the Netherlands Organisation for Scientific Research (NWO). The authors would like to thank P. Planken for useful discussions.

Appendix A. Model photoconductive switch and electrical circuit

Here we describe a model of the electrical circuit and photoconductive switch, in order to calculate the time-dependent voltage over the deflector. For the model a set of differential equations is derived describing the time-dependent voltages in the system as function of parameters like the deflector capacitance and laser pulse energy. The results are shown in Fig. 8 of Section 6.

In the model it is assumed that the currents in the UFB can be described by basic circuit laws, valid because the dimensions are significantly smaller than the wavelength. Fig. 10 shows the electrical circuit used for the model. We assume a constant voltage at the source, V_s, connected via a transmission line to the photoconductive switch. The transmission line is simplified as a combination of a capacitor and inductor.

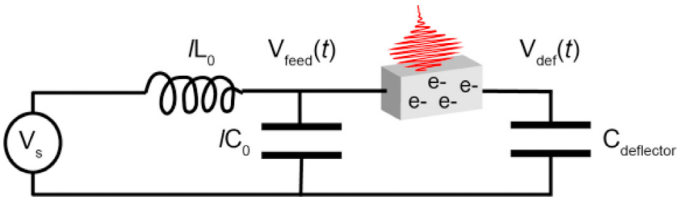

Fig. 10. Scheme of the electric circuit. A laser pulse illuminates the photoconductive switch which has a length L and cross area A and generates a free carrier density $n(t)$. The carriers accelerate in the field, according to a Drude–Lorentz model, the average velocity, $v(t)$, of the electrons is considered positive when they move to the left in this figure.

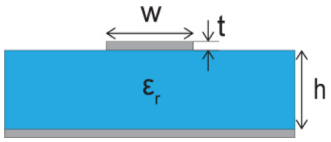

Fig. 11. Microstrip line with electrode separation h, in our case 1 μm, the width, w, is equal to 30 μm. The dielectric has a relative permittivity ε_r.

The capacitance and inductance in Fig. 10, L_0 and C_0, are estimated by assuming the electrodes are like a micro strip line. The characteristic impedance Z_0 of a microstrip line is estimated using the equations in Demarest [47]:

$$\varepsilon_{eff} \approx \tfrac{1}{2}(\varepsilon_r + 1) + \tfrac{1}{2}(\varepsilon_r - 1)\left(1 + 12\frac{w}{h}\right)^{-1/2}$$
$$Z_0 \approx \frac{120\pi}{\sqrt{\varepsilon_{eff}}}\left[\frac{w}{h} + 1.393 + 0.667\ln\left(\frac{w}{h} + 1.444\right)\right]^{-1} \quad (18)$$

This equation is valid for $w/h > 1$, all variables are defined in Fig. 11. For the relative permittivity we take the average of glass and GaAs which have refractive indices of 1.5 and 3.4 respectively. In our design the characteristic impedance is equal to 4.3 Ω.

The capacitance per unit length is calculated under the assumption of a simple 2 plate capacitor, with the dimensions indicated in Fig. 11 and is equal to 1.9 nF/m. From the capacitance and impedance the inductance per unit length is calculated using $L_0 = Z_0^2 C_0$ and is equal to 36 nH/m.

In the following section we use Kirchhoff's current law at the feed plate and deflector plate to derive two higher order ordinary differential equations. The differential equations are rewritten in a set of first order ordinary differential equations which are numerically solved with Matlab.

The sum of the currents at the feed plate has to be equal to zero:

$$\frac{1}{L_f}\int \left(V_s - V_f\right)dt - C_0\frac{dV_f}{dt} - eAn(t)v(t) = 0 \quad (19)$$

The first term describes the effect of the coil, included in the model because the source can't instantaneously deliver new charges to the feed plate. The next term describes the current flowing from the feed plate due to its capacitance. The last term describes the current flowing into the photoconductive switch. Which is determined by the amount of carriers generated by the laser pulse and the average velocity, $v(t)$. Differentiating this equation to time, in order to get rid of the integral, gives:

$$\frac{\left(V_s - V_f\right)}{L_0} - C_0\frac{d^2V_f}{dt^2} - eA\left(v\frac{dn}{dt} + n\frac{dv}{dt}\right) = 0 \quad (20)$$

The velocity is described with a Drude–Lorentz model given in Eq. (2), which has an additional term to correct for the reduction in average velocity due to the newly generated free carriers at later time instances [38]:

$$\frac{dv}{dt} = \frac{e}{m*}E - \frac{v}{\tau_s} - v\frac{dn/dt}{n} \quad (21)$$

where n is the density of charges, proportional to the integral of a Gaussian shaped laser pulse:

$$n(t) = \tfrac{1}{2}n_0\left(1 + erf\left[1.67\frac{t - t_0}{\tau}\right]\right) \quad (22)$$

where n_0 is the total amount of carriers generated by the laser pulse, t_0 is the time the laser pulse illuminates the photoconductive switch and τ is the FWHM laser pulse length. Recombination of electron-hole pairs is not taken into account because it happens at a time scale of 10–15 ps.

Inserting Eq. (21) in Eq. (20) results in the following equation:

$$\frac{\left(V_s - V_f\right)}{L_0} - C_0\frac{d^2V_f}{dt^2} - eA\left(\frac{ne}{Lm^*}\left(V_f - V_d\right) - \frac{nv}{\tau_s}\right) = 0 \quad (23)$$

Combining this equation with (19) by replacing the term $n(t)v(t)$ and differentiating to time:

$$-\frac{1}{L_f}\frac{dV_f}{dt} - C_0\frac{d^3V_f}{dt^3} - \frac{Ae^2}{Lm^*}\left(\frac{dV_f}{dt} - \frac{dV_d}{dt}\right)n - \frac{Ae^2}{Lm^*}\left(V_f - V_d\right)\frac{dn}{dt}$$
$$+\frac{1}{L_f\tau_s}\left(V_s - V_f\right) - \frac{C_0}{\tau_s}\frac{d^2V_f}{dt^2} = 0 \quad (24)$$

We now have a differential equation independent of the velocity, v, describing the voltage at the feed plate V_f. A second equation is required because there are still two unknowns, V_f and V_d.

A second differential equation is derived by applying Kirchhoff's circuit rule at the deflector plate:

$$C_d\frac{dV_d}{dt} - eAnv = 0 \quad (25)$$

Differentiating this equation to time gives:

$$C_d\frac{d^2V_d}{dt^2} - eA\left(n\frac{dv}{dt} + v\frac{dn}{dt}\right) = 0 \quad (26)$$

Inserting Eq. (21) in Eq. (26) results in:

$$C_d\frac{d^2V_d}{dt^2} - eA\left(n\frac{e}{m*}E - \frac{nv}{\tau_s} - vdn/dt + v\frac{dn}{dt}\right) = 0$$
$$C_d\frac{d^2V_d}{dt^2} - eA\left(n\frac{e}{m*}\frac{V_f - V_d}{L} - \frac{nv}{\tau_s}\right) = 0$$
$$\frac{d^2V_d}{dt^2} = \frac{e^2An}{LC_dm*}\left(V_f - V_d\right) - \left(\frac{1}{\tau_s}\right)\frac{dV_d}{dt} \quad (27)$$

With 2 differential equations and 2 unknowns it is possible to numerically calculate the voltages as function of time. In order to solve the set of differential equations numerically, using MATLAB, we rewrite it in a set of first order differential equations, where we define:

$$v(1) = V_d$$
$$v(2) = \frac{dV_d}{dt}$$
$$v(3) = V_f$$
$$v(4) = \frac{dV_f}{dt}$$
$$v(5) = \frac{d^2V_f}{dt^2} \quad (28)$$

The set of coupled first order differential equations we solved in MATLAB are:

$$
\begin{aligned}
v'(1) &= v(2)\\
v'(2) &= \frac{\alpha n}{C_d}(v(3)-v(1)) - \frac{1}{\tau_s}v(2)\\
v'(3) &= v(4)\\
v'(4) &= v(5)\\
v'(5) &= -\frac{1}{\tau_f^2}v(4) - \frac{\alpha n}{C_f}[v(4)-v(2)] - \frac{\alpha}{C_f}[v(3)-v(1)]\frac{dn}{dt}\\
&\quad + \frac{1}{\tau_s\tau_f^2}[V_s - v(3)] - \frac{1}{\tau_s}v(5)
\end{aligned}
\tag{29}
$$

where:

$$
\alpha = \frac{e^2 A}{m^* L}, \tau_f^2 = C_f L_f \tag{30}
$$

A value of 1.9 nF/m and 35 nH/m is used for respectively the capacitance and inductance of the feed plate. We use a length, L_f, of 10 µm for the transmission line. The cross section A is equal to 10 µm^2, L is equal to 10 µm and the effective mass is 0.067m$_0$, where m$_0$ is equal to the electron rest mass. A value of 6 fF is used for the capacitance of the deflector plate. The electron scatter time is taken to be equal to 30 fs, corresponding to a mobility of 786 cm^2/V·s.

References

[1] R.M. Van Der Veen, O. Kwon, A. Tissot, A. Hauser, A.H. Zewail, Single-nanoparticle phase transitions visualized by four-dimensional electron microscopy, Nat. Chem. (2013) 1–8, doi:10.1038/NCHEM.1622.

[2] D.-S. Yang, O.F. Mohammed, A.H. Zewail, Environmental scanning ultrafast electron microscopy: structural dynamics of solvation at interfaces, Angew. Chem. Int. Ed. Engl. 52 (2013) 2897–2901, doi:10.1002/anie.201205093.

[3] B. Barwick, D.J. Flannigan, A.H. Zewail, Photon-induced near-field electron microscopy, Nature 462 (2009) 902–906, doi:10.1038/nature08662.

[4] A. Yurtsever, R.M. van der Veen, A.H. Zewail, Subparticle ultrafast spectrum imaging in 4D electron microscopy, Science 335 (2012) 59–64, doi:10.1126/science.1213504.

[5] A. Feist, K.E. Echternkamp, J. Schauss, S.V. Yalunin, S. Schäfer, C. Ropers, Quantum coherent optical phase modulation in an ultrafast transmission electron microscope, Nature 521 (2015) 200–203, doi:10.1038/nature14463.

[6] A. Ryabov, P. Baum, Electron microscopy of electromagnetic waveforms, Science 2182 (2016) 2179–2182.

[7] K.E. Echternkamp, A. Feist, S. Schäfer, C. Ropers, Ramsey-type phase control of free-electron beams, Nat. Phys. 12 (2016) 1000–1004, doi:10.1038/nphys3844.

[8] A.H. Zewail, Four-dimensional electron microscopy, Science 328 (2010) 187–193, doi:10.1126/science.1166135.

[9] B. Barwick, H. Soon Park, O.-H. Kwon, J.S. Baskin, A.H. Zewail, 4D imaging of transient structures and morphologies in ultrafast electron microscopy, Science 369 (2008) 1227–1232, doi:10.1007/978-1-59745-294-6.

[10] V.A. Lobastov, R. Srinivasan, A.H. Zewail, Four-dimensional ultrafast electron microscopy, Proc. Natl. Acad. Sci. U. S. A. 102 (2005) 7069–7073, doi:10.1073/pnas.0502607102.

[11] P. Hommelhoff, C. Kealhofer, M.A. Kasevich, Ultrafast electron pulses from a tungsten tip triggered by low-power femtosecond laser pulses, Phys. Rev. Lett. 97 (2006) 247402, doi:10.1103/PhysRevLett.97.247402.

[12] D.-S. Yang, O.F. Mohammed, A.H. Zewail, Scanning ultrafast electron microscopy, Proc. Natl. Acad. Sci. U. S. A. 107 (2010) 14993–14998, doi:10.1073/pnas.1009321107.

[13] B. Cook, P. Kruit, Coulomb interactions in sharp tip pulsed photo field emitters, Appl. Phys. Lett. 109 (2016) 151901, doi:10.1063/1.4963783.

[14] A. Feist, N. Bach, N. Rubiano da Silva, T. Danz, M. Möller, K.E. Priebe, T. Domröse, J.G. Gatzmann, S. Rost, J. Schauss, S. Strauch, R. Bormann, M. Sivis, S. Schäfer, C. Ropers, Ultrafast transmission electron microscopy using a laser-driven field emitter: femtosecond resolution with a high coherence electron beam, Ultramicroscopy 176 (2017) 63–73, doi:10.1016/j.ultramic.2016.12.005.

[15] D. Ehberger, J. Hammer, M. Eisele, M. Krüger, J. Noe, A. Högele, P. Hommelhoff, Highly Coherent Electron Beam from a Laser-Triggered Tungsten Needle Tip, Phys. Rev. Lett. 114 (2015) 1–5, doi:10.1103/PhysRevLett.114.227601.

[16] L.C. Oldfield, A rotationally symmetric electron beam chopper for picosecond pulses, J. Phys. E 9 (1976) 455–463, doi:10.1088/0022-3735/9/6/011.

[17] T. Hosokawa, H. Fujioka, K. Ura, Generation and measurement of subpicosecond electron beam pulses, Rev. Sci. Instrum. 49 (1978) 624, doi:10.1063/1.1135464.

[18] K. Ura, H. Fujioka, T. Hosokawa, Picosecond pulse stroboscopic scanning electron microscope, J. Electron Microsc. 27 (1978) 247–252 (Tokyo).

[19] M. Brunner, D. Winkler, B. Lischke, Electron-beam test system for high-speed devices, 9 (1987) 201–204.

[20] A.C. Lassise, Miniaturized RF Technology for Femtosecond Electron Microscopy, Eindhoven University of Technology, 2012.

[21] J.F.M. van Rens, W. Verhoeven, J.G.H. Franssen, A.C. Lassise, X.F.D. Stragier, E.R. Kieft, P.H.A. Mutsaers, O.J. Luiten, Theory and particle tracking simulations of resonant, radio frequency cavities in TM110 mode as dynamic electron-optical elements for ultrafast electron microscopy, (2017). http://www.sciencedirect.com/science/article/pii/S0304399117303339?_rdoc=1&_fmt=high&_origin=gateway&_docanchor=&md5=b8429449ccfc9c30159a5f9aeaa92ffb.

[22] W. Verhoeven, E.R. Kieft, O.J. Luiten, High quality ultrafast transmission electron microscopy using resonant microwave cavities, arXiv. (2017).

[23] G.J.H. Brussaard, A. Lassise, P.L.E.M. Pasmans, P.H.A. Mutsaers, M.J. van der Wiel, O.J. Luiten, Direct measurement of synchronization between femtosecond laser pulses and a 3 GHz radio frequency electric field inside a resonant cavity, Appl. Phys. Lett 103 (2013) 141105, doi:10.1063/1.4823590.

[24] A. Gliserin, M. Walbran, P. Baum, Passive optical enhancement of laser-microwave synchronization, Appl. Phys. Lett 103 (2013) 1–5, doi:10.1063/1.4815929.

[25] P. Kruit, I.G.C. Weppelman, Device and Method for Generating Charged Particle Beam Pulses, WO2016076718 A3, 2016.

[26] J.T.L. Thong, Picosecond electron pulse generation via beam deflection-chopping in the SEM, Meas. Sci. Technol. (1991) 207–216.

[27] D.H. Auston, P. Lavallard, N. Sol, D. Kaplan, An amorphous silicon photodetector for picosecond pulses, Appl. Phys. Lett 36 (1980) 66, doi:10.1063/1.91276.

[28] T. Motet, J. Nees, S. Williamson, G. Mourou, 1.4 ps rise-time high-voltage photoconductive switching, Appl. Phys. Lett. 59 (1991) 1455–1457.

[29] Y. Chiu, S.B. Fleischer, D. Lasaosa, J.E. Bowers, Ultrafast (370 GHz bandwidth) using low-temperature-grown GaAs p-i-n traveling wave photodetector using low-temperature-grown GaAs, Appl. Phys. Lett. 71 (1997) 2508–2510, doi:10.1063/1.120115.

[30] C.A. Schmuttenmaer, Exploring dynamics in the far-infrared with terahertz spectroscopy, Chem. Rev. 104 (2004) 1759–1779, doi:10.1021/cr020685g.

[31] G.H. Kassier, K. Haupt, N. Erasmus, E.G. Rohwer, H.M. Von Bergmann, H. Schwoerer, S.M.M. Coelho, F.D. Auret, A compact streak camera for 150 fs time resolved measurement of bright pulses in ultrafast electron diffraction, Rev. Sci. Instrum 81 (2010), doi:10.1063/1.3489118.

[32] J. Feng, H.J. Shin, J.R. Nasiatka, W. Wan, A.T. Young, G. Huang, A. Comin, J. Byrd, H.A. Padmore, An x-ray streak camera with high spatio-temporal resolution, Appl. Phys. Lett 91 (2007) 134102, doi:10.1063/1.2793191.

[33] A.M. Johnson, D.H. Auston, P.R. Smith, J.C. Bean, J.P. Harbison, A.C. Adams, Picosecond transient photocurrents in amorphous silicon, Phys. Rev. B. 23 (1981) 6816–6819, doi:10.1103/PhysRevB.23.6816.

[34] M.C. Beard, G.M. Turner, C.A. Schmuttenmaer, Subpicosecond carrier dynamics in low-temperature grown GaAs as measured by time-resolved terahertz spectroscopy, J. Appl. Phys. 90 (2001) 5915, doi:10.1063/1.1416140.

[35] P.U. Jepsen, R.H. Jacobsen, S.R. Keiding, Generation and detection of terahertz pulses from biased semiconductor antennas, J. Opt. Soc. Am. B 13 (1996) 2424, doi:10.1364/JOSAB.13.002424.

[36] A.V. Kuznetsov, C.J. Stanton, Ultrafast optical generation of carriers in a dc electric field: transient localization and photocurrent, Phyiscal Rev. B 48 (1993) 10828–10845.

[37] B.B. Hu, A.S. Weling, D.H. Auston, A.V. Kuznetsov, C.J. Stanton, dc-electric-field dependence of THz radiation induced by femtosecond optical excitation of bulk GaAs, Phys. Rev. B. 49 (1994) 2234–2237.

[38] H. Ne̊mec, A. Pashkin, P. Kuzȩl, M. Khazan, S. Schnuĺl, I. Wilke, Carrier dynamics in low-temperature grown GaAs studied by terahertz emission spectroscopy, J. Appl. Phys. 90 (2001) 1303–1306, doi:10.1063/1.1380414.

[39] J. Požela, A. Reklaitis, Electron transport properties in GaAs at high electric fields, Solid. State. Electron 23 (1980) 927–933, doi:10.1016/0038-1101(80)90057-X.

[40] P. Kruit, M. Bezuijen, J.E. Barth, Source brightness and useful beam current of carbon nanotubes and other very small emitters, J. Appl. Phys. 99 (2006), doi:10.1063/1.2162270.

[41] H. Nyquist, Thermal agitation of electric charge in conductors, Phys. Rev. 32 (1928) 110–113, doi:10.1103/PhysRev.32.110.

[42] R. Sarpeshkar, T. Delbruck, C.A. Mead, White noise in MOS transistors and resistors, IEEE Circ. Devices Mag. 9 (1993) 23–29, doi:10.1109/101.261888.

[43] A.H.V. van Veen, C.W. Hagen, J.E. Barth, P. Kruit, Reduced brightness of the ZrO/W Schottky electron emitter, J. Vac. Sci. Technol. B Microelectron. Nanom. Struct. 19 (2001) 2038, doi:10.1116/1.1409390.

[44] A. Lassise, P.H.A. Mutsaers, O.J. Luiten, Compact, low power radio frequency cavity for femtosecond electron microscopy, Rev. Sci. Instrum. 83 (2012) 43705, doi:10.1063/1.3703314.

[45] W. Verhoeven, J.F.M. van Rens, M.A.W. van Ninhuijs, W.F. Toonen, E.R. Kieft, P.H.A. Mutsaers, O.J. Luiten, Time-of-flight electron energy loss spectroscopy using TM110 deflection cavities, Struct. Dyn. 3 (2016) 54303, doi:10.1063/1.4962698.

[46] R.J. Moerland, I.G.C. Weppelman, W.H. Garming, P. Kruit, J.P. Hoogenboom, Time-resolved cathodoluminescence microscopy with sub-nanosecond beam blanking for direct evaluation of the local density of states, Opt. Express 24 (2016) 499–504.

[47] K.R. Demarest, Engineering Electromagnetics, Prentice Hall, 1998.